CHEMISTRY

Abiotic molecular oxygen production—Ionic pathway from sulfur dioxide

Måns Wallner[1], Mahmoud Jarraya[2,3], Emelie Olsson[1], Veronica Ideböhn[1], Richard J. Squibb[1], Saida Ben Yaghlane[2], Gunnar Nyman[4], John H.D. Eland[5], Raimund Feifel[1]*, Majdi Hochlaf[3]*

Molecular oxygen, O_2, is vital to life on Earth and possibly also on exoplanets. Although the biogenic processes leading to its accumulation in Earth's atmosphere are well understood, its abiotic origin is still not fully established. Here, we report combined experimental and theoretical evidence for electronic state–selective production of O_2 from SO_2, a chemical constituent of many planetary atmospheres and one that played an important part on Earth in the Great Oxidation Event. The O_2 production involves dissociative double ionization of SO_2 leading to efficient formation of the O_2^+ ion, which can be converted to abiotic O_2 by electron neutralization or by charge exchange. This formation process may contribute substantially to the abundance of O_2 and related ions in planetary atmospheres, such as the Jovian moons Io, Europa, and Ganymede. We suggest that this sort of ionic pathway for the formation of abiotic O_2 involving multiply charged molecular ion decomposition may also exist for other atmospheric and planetary molecules.

INTRODUCTION

Molecular oxygen, O_2, is closely connected to life on Earth and has a decisive role in the oxidation state of the other elements. Before becoming stabilized, the O_2 concentration in the Earth atmosphere increased strongly during the Great Oxidation Event, which occurred ~2.4 billion years ago (*1*). Although the biogenic processes leading to its accumulation in the atmosphere are well understood, its abiotic origin is still not fully established. In primitive Earth, the commonly admitted models assume that O_2 is formed through the three-body recombination reaction $O + O + M \rightarrow O_2 + M$, where the O atoms are produced by photolysis of CO_2 or other molecules (*1*–*4*). It was also suggested that abiotic O_2 may be produced efficiently through photodissociation of water vapor by extreme ultraviolet (XUV) light (*5*–*7*) or the near-ultraviolet (NUV) photochemistry of titanium (IV) oxide (titania) (*8*). In addition to these bi- and plurimolecular processes, the pioneering work of Lu and co-workers from 2014 (*9*) showed that unimolecular decomposition reactions can lead to O_2. These authors provided evidence that state-selective vacuum ultraviolet (VUV) photodissociation of CO_2 can provide O_2 with 5% efficiency. Similarly, recent studies suggest that most of the O_2 in Europa's exosphere is produced by UV photolysis of H_2O vapor (*10*). Also, Li and co-workers (*11*) most recently recorded a related pathway for the formation of $S_2 + C$ after CS_2 VUV photodissociation. In 2016, Wang and co-workers (*12*) provided experimental evidence for a channel of dissociative electron attachment to CO_2 that produces $O_2 + C^-$.

O_2^+ is the most abundant molecular ion in the ionosphere of Venus. As explanation, the fast exothermic reaction $O^+ + CO_2 \rightarrow O_2^+ + CO$, where the O^+ ions are released from dissociative ionization of CO_2, is proposed (*13*). However, this mechanism cannot play a role in media where CO_2 is absent or has a low concentration such as in the atmospheres of the Jovian moons Io, Europa, and Ganymede. Sulfur dioxide (SO_2) is dominant at more than 90% in the atmosphere of Io (*14*–*16*) and might play a role in processes leading to O_2.

On Earth, SO_2 has both anthropogenic and natural origins, and is involved in the formation of environmental pollutants [e.g., sulfuric acid or sulfuric acid aerosols (*17*)], contributing to related deleterious effects such as acid rains and smogs. During the Great Oxidation Event (*1*), SO_2 strongly influenced Earth's first sulfur cycle through its participation in gas phase reactions resulting in fixing the oxidation state of sulfur (*18*). Moreover, it drives the geochemical cycle of sulfur in Mars's, Venus's, Io's, and conjecturally on some terrestrial exoplanets' atmospheres (*16*, *19*–*22*), leading, for instance, to high SO_2 concentrations in the atmospheres of Venus and Io (*23*) mainly due to outgassing from volcanism. Consequently, SO_2 is proposed as a proxy for volcanic activity on extrasolar planets (*24*). In addition, SO_2 may have played a role in the emergence of life on Earth either directly or indirectly by contributing to O_2 formation in the form of abiotic processes. It was suggested recently that SO_2 clouds emitted from erupting volcanoes may have kick-started chemical processes that led to the emergence of life on Earth more than 4 billion years ago (*25*).

While its role in the formation of sulfur-containing compounds is relatively well understood, the involvement of SO_2 in the production of other major components such as O_2 and O_2^+ in the atmospheres of Earth, Venus, or Io is not. For neutral SO_2, ultrafast photodissociation dynamics studies induced by intense ultrashort laser pulses in a pump-probe scheme evoked the idea that an intermediate fast-rotating O_2 molecule might be formed before complete fragmentation (*26*), but no O_2 production from SO_2 was revealed by these experiments.

The present work, combining single-photon ionization and advanced ab initio computations, shows that dissociative double ionization of SO_2 produces O_2^+, which after neutralization may form abiotic O_2. This can be regarded as the first experimental evidence of an ionic pathway for the formation of O_2 in abiotic media. In the

[1]University of Gothenburg, Department of Physics, Origovägen 6B, 412 58 Gothenburg, Sweden. [2]Université de Tunis El Manar, Faculté des Sciences de Tunis, Laboratoire de Spectroscopie Atomique, Moléculaire et Applications—LSAMA, 2092 Tunis, Tunisia. [3]Université Gustave Eiffel, COSYS/IMSE, 5 Bd Descartes, 77454 Champs sur Marne, France. [4]University of Gothenburg, Department of Chemistry and Molecular Biology, Kemigården 4, 412 96 Gothenburg, Sweden. [5]Oxford University, Department of Chemistry, Physical and Theoretical Chemistry Laboratory, South Parks Road, Oxford OX1 3QZ, UK.
*Corresponding author. Email: raimund.feifel@physics.gu.se (R.F.); majdi.hochlaf@univ-eiffel.fr (M.H.)

present-day atmosphere of Io and the primitive atmospheres of Earth and Venus, ionic pathways from SO_2 to O_2 are certainly plausible since those media are strongly bombarded by ionizing radiation where single, double, and inner shell ionizations are very likely to occur. While the atmosphere on Earth is primarily dominated by nitrogen and oxygen whose inner shells lie at very high energy with low cross section, sulfur, because of its 2p shell, has a much larger cross section for double ionization involving the Auger route at much lower energy. In the context of the formation of O_2^+ from SO_2^{2+}, our calculations show that the less stable nonlinear SO_2^{2+} and especially OOS^{2+} isomers play crucial roles. The OSO^{2+} isomer is linear in its ground state with two nonadjacent O atoms, whereas the two O atoms are directly bound to each other in OOS^{2+}. This is substantiated by mapping the potential energy surfaces (PESs) of OSO^{2+} and OOS^{2+} to yield insights into the formation mechanism of O_2^+ by state-selective double ionization of SO_2.

SO_2 has been investigated experimentally in the present work and in the past (*27*) by multiparticle coincidence detection using the TOF-PEPEPIPICO (time-of-flight photoelectron-photoelectron-photoIon-photoIon coincidence) technique where the target species were irradiated by 40.81-eV photons (HeIIα) from a pulsed helium discharge lamp, mimicking an intense component of the solar spectrum and of many stellar spectra. In addition, ion-ion coincidence measurements on SO_2 were carried out at the synchrotron radiation facility BESSY-II where photon energies of several more solar x-ray lines were available to us.

From previous studies [see (*28*) and references therein], it is known that upon double ionization SO_2 dissociates following four principal channels

$$SO_2^{2+} \rightarrow O^+ + SO^+ \quad (1)$$

$$SO_2^{2+} \rightarrow O^+ + S^+ + O \quad (2)$$

$$SO_2^{2+} \rightarrow O_2^+ + S^+ \quad (3)$$

$$SO_2^{2+} \rightarrow O + SO^{2+} \quad (4)$$

A fifth channel producing two O^+ and a neutral S species is detectable but of negligible intensity. The other dissociative channels have been discussed in a previous publication (*28*), but here, we concentrate entirely on the formation of molecular oxygen ions.

RESULTS

The $SO_2^{2+} \rightarrow O_2^+ + S^+$ channel is embedded in a dense manifold of dissociation limits forming $SO^+ + O^+$ and $SO^{2+} + O$ products in their electronic ground states (see table S1). Standard unimolecular reaction rate theory indicates that the simple OS—O bond breaking reaction leading to the $SO^+ + O^+$ fragments, which has the lowest appearance energy [34 eV; (*29*)], should be strongly favored over all channels with higher energy requirements. In contrast, we demonstrate here that despite its higher appearance energy [ca. 36 eV (*29*)], the O_2^+ product is formed efficiently by a state-selective dissociation of SO_2^{2+} involving a nuclear rearrangement; O_2^+ can then form O_2 by electron recombination or by charge exchange. Besides the importance of this finding for the abiotic generation of O_2, the new mechanism proposed here may apply widely in dissociations of doubly and multiply ionized molecules.

Figure 1A shows an electron pair spectrum extracted in correlation with either O_2^+ or S^+ ions from threefold coincidence events, as well as an electron pair spectrum extracted in correlation with both the O_2^+ and S^+ ions from fourfold events. These two spectra were obtained under identical conditions. For comparison, a higher-resolution electron pairs–only spectrum that reflects the total double ionization at the same photon energy, previously discussed in (*27*), is shown. The ion fragmentation curves are displaced horizontally on a common scale (with fixed offsets) and show true relative intensities, while the overall spectrum included for comparison has an intensity scale adjusted for display. The horizontal bar combs mark MRCI/aug-cc-pV(Q+d)Z computed vertical double-ionization energies of SO_2 quoted for C_{2v} symmetry as given in (*28*).

Figure 1B presents an estimate of the branching ratios of SO_2 for the experimentally detectable dissociative double-ionization channels at 40.81-eV photon energy. For the channels involving two ionic fragments, fourfold coincidences are used, and for the channel containing $O + SO^{2+}$, threefold coincidences are used. In particular, this figure shows the channel leading to the $O_2^+ + S^+$ formation of interest in the present work.

Figure 1C shows the isomers of SO_2^{2+}. Because all the isomers appear at energies well below the appearance energy of $O_2^+ + S^+$, they are all possible candidates from which the dissociation can occur. Linear OSO^{2+} was already identified in (*27*), whereas bent OSO^{2+}

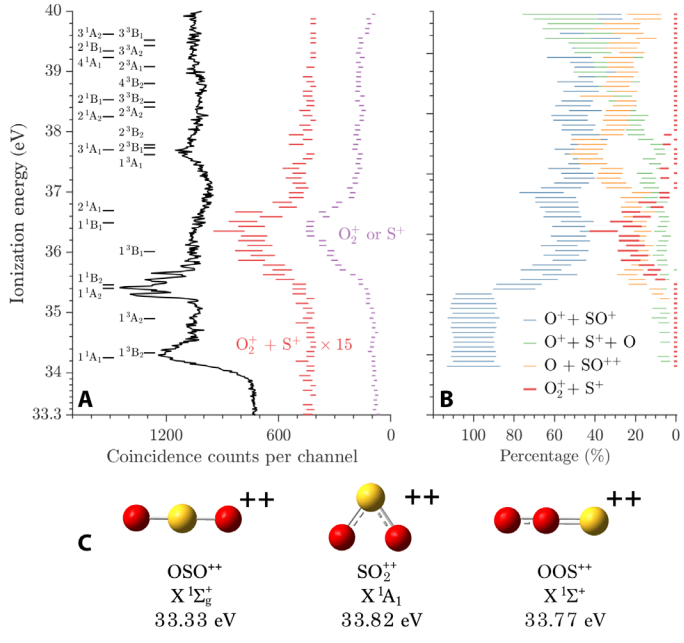

Fig. 1. Electron coincidence spectra and breakdown diagrams of doubly ionized SO_2. (**A**) Electron pairs measured in coincidence with two ions in red (from fourfold events) and one ion in purple (from threefold events) upon photoionization of SO_2 at 40.81-eV photon energy. For comparison, the black curve is a higher-resolution electron pair–only spectrum of the total double ionization at the same photon energy previously discussed in (*27*). The bar combs mark the vertical ionization energies computed at the MRCI/aug-cc-pV(Q+d)Z level of theory at the neutral SO_2 ($X\,^1A_1$) ground-state equilibrium geometry, i.e., at an O—S—O angle of 120° and SO distance of 2.7 bohr [see (*28*) for more details]. (**B**) Breakdown diagram of the major detectable decay channels of doubly ionized SO_2. (**C**) Metastable isomers of SO_2^{2+}, which are accessible in the energy region where $O_2^+ + S^+$ is detectable. We give their relative energies with respect to the SO_2 ($X\,^1A_1$) vibrationless level.

and OOS^{2+} are identified here, although neutral OOS in solid argon was already characterized by Lee and co-workers (*30*) using infrared spectroscopy. In the context of the formation of O_2^+ from SO_2^{2+}, the less stable bent SO_2^{2+} and especially OOS^{2+} isomers should play crucial roles. OSO^{2+} is linear in its ground state with two nonadjacent O atoms, whereas the two O atoms are bound in OOS^{2+}. Therefore, we mapped the PESs of OSO^{2+} and those of OOS^{2+} to shed light onto the formation mechanisms of O_2^+ by state-selective double ionization of SO_2 (see figs. S2 to S9 for more details).

Insights into the fragmentation mechanisms can be obtained from the kinetic energy releases (KERs). The magnitudes of the KERs in the different dissociation channels can be extracted from the width and shape of the ion TOF peaks, and for the charge-separating channels of doubly ionized SO_2, this has been done several times before (*31*–*36*) with generally concordant results, but without initial state selection. The most detailed measurements, made possible by use of a position-sensitive ion detector, gave the full KER distributions for 40.81-eV photoionization (*36*). For the two-body dissociation producing $O_2^+ + S^+$, the distribution is quite narrow [full width at half maximum (FWHM) ≈ 2 eV] and centered at about 5 eV. Field and Eland (*29*) determined energy releases as a function of the maximum (double) ionization energy for all four major dissociation channels of SO_2^{2+} using single-electron-ion(-ion) coincidences. For the main two-body charge separation, the energy release was found to vary slightly, between 4.3 ± 0.5 and 5.2 ± 0.5 eV over the range of ionization energies of 34 to 40 eV. Because we collect and analyze both electrons, we can now determine mean KERs as a function of the actual energies transferred in double ionization, which is an important aspect of the present work.

As can be seen from Fig. 1, the channel leading to $O_2^+ + S^+$ arises specifically from states in the energy range between 35.5 and 36.8 eV where the $^3B_1$, $^1B_1$, $^1B_2$, and 2 $^1A_1$ states are found to be located (*27*). Its peak intensity occurs at about 36.5-eV ionization energy with an onset at about 35.3 eV, energies that are well above the thermodynamic threshold of 28.4 eV for the ground-state $O_2^+ + S^+$ products. There is a broad feature in the overall double-ionization spectrum at exactly the same energy. If the mean KER of 6 eV (*31*) or 5.6 eV (*36*) is added to the ground-state product energy, the resulting calculated threshold is 34.3 or 33.9 eV, i.e., below the observed onset. This suggests that the fragments are formed with substantial internal energy. The KER appears from our data to be slightly lower than the values reported by Curtis and Eland (6 ± 1 eV) (*31*) and Hsieh and Eland (peak at 5.4 eV) (*36*), where the values known in the literature reflect kinetic energies from the whole range of dication electronic states accessed at 40.81 eV. The experimental value from the present work that we consider most reliable (because of the greater selectivity available here in comparison to previous works) is 4.7 ± 0.3 eV for the ionization energy range of 36.3 to 36.8 eV where these products are formed most abundantly. When subtracted from the mean ionization energy of 36.5 eV, this places the energy of the products at 31.8 eV, well above the thermodynamic limit of 28.4 eV for the formation of $O_2^+ + S^+$ ground-state products. The implied internal excitation energy of 3.4 eV could easily be accommodated, for instance, as vibrational energy of the O_2^+ ion.

To further examine the dissociation producing $O_2^+ + S^+$, we have performed ab initio computations of the PESs of the singlet and triplet electronic states located in the 32- to 42-eV energy range above the neutral SO_2 ($X\ ^1A_1$) ground state. These PESs were mapped over a wide range of nuclear configurations covering the molecular regions, where we locate the SO_2^{2+} isomers, and the dissociation asymptotes. For instance, panels A and B of Fig. 2 show several sets of PES cuts, and panel C presents the thermodynamic thresholds for $O_2^+ + S^+$. The PESs in Fig. 2 are computed in Jacobi coordinates where the position of the sulfur atom is varied along the coordinates R ∈ [0.5,5] (Å) and θ ∈ [0,90] (°) relative to the center of mass of O_2 (see the Supplementary Materials for more details). The oxygen atoms are separated by the equilibrium distance of the neutral SO_2 (X^1A_1) ground state. The PES computations were done at the CASSCF/MRCI/aug-cc-pV(Q+d)Z level of theory. Thermodynamic threshold computations were done at the (R)CCSD(T)/CBS level for comparison with the precise thresholds known from thermochemical heats of formation and spectroscopic information.

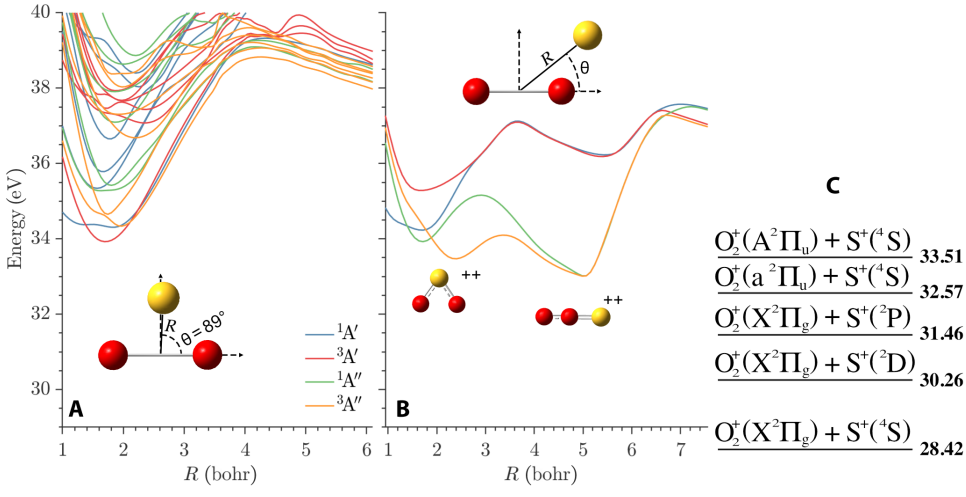

Fig. 2. Potential energy surface cuts and minimum energy paths of the lowest electronic states of SO_2^{2+} for varying bond distance of S. (**A**) One-dimensional PES cuts of the lowest states of SO_2^{2+} for the in-plane angle θ = 89° along the bond distance of S to the center of mass of O_2, where the O_2 distance is kept fixed at its value in the neutral SO_2 ($X\ ^1A_1$) ground-state equilibrium geometry (i.e., 4.6 bohr). (**B**) Corresponding MEP for bent SO_2^{2+} and O—O—S^{2+}. (**C**) Thermodynamic thresholds of $O_2^+ + S^+$. The reference energy is that of SO_2 ($X\ ^1A_1$) in its vibrationless ground state. Other cuts are given in figs. S2 to S5.

The curves in Fig. 2A demonstrate that the potential energy threshold toward dissociation is much too high (~39 eV), suggesting that the sulfur atom does not leave the system in this way. The vast number of states presented in this panel motivates a minimum energy path (MEP) analysis. This is done by following the valley bottom in the PES as the sulfur atom is moved out in the Jacobi coordinate system. In the present analysis, the O—O distance is kept fixed, thus providing the reduced MEP. In Fig. 2B, the reduced (fixed O—O distance) MEP of the $^1A'$, $^1A''$, $^3A'$, and $^3A''$ PESs is shown, where the angle θ giving the minimal energy is selected for each R. This MEP has an odd shape (far from the usual Morse-like potentials) favoring large-amplitude motions and intramolecular isomerizations to take place. For instance, the MEP analysis suggests a roaming pathway where SO_2^{2+} may convert from a bent OSO^{2+} configuration to a linear OOS^{2+} isomer by crossing a potential barrier at about 34.5 eV. This roaming mechanism is further demonstrated in Fig. 3, which is computed in the coordinate system where one oxygen atom is moved relative to the other oxygen atom by varying the angle φ with the bond distance fixed at 5.3 bohr, corresponding to the equilibrium distance in the SO_2^{2+} ($X^1\Sigma_g^+$) ground state. Figure 3 shows the roaming from a linear OSO^{2+}, crossing the barrier at 34.4 eV by spin-orbit conversion from the $^1A'$ to the $^3A''$ state. Such a roaming O_2 molecular mechanism was recently reported by Lin and co-workers (*26*), who studied the ultrafast photodissociation dynamics of neutral SO_2, induced by intense ultrashort laser pulses. Their pump-probe experiments indicated that an intermediate fastly rotating O_2 molecule is formed before complete fragmentation. Nevertheless, there was no O_2 production from SO_2 detected in those experiments, most likely because the O_2 molecule carries enough excess energy to dissociate.

Figure 4 displays PES cuts computed in the coordinate system where one oxygen atom is moved relative to the other oxygen atom by varying the angle τ, while the SO bond is fixed to 5.1 bohr from the equilibrium of the OOS^{2+} ($X^1\Sigma^+$) ground state. The figure illustrates how the formation of O_2^+ can go through the formation of the OOS^{2+} isomer, i.e., after O roaming, since the two O atoms are far away in ground-state OSO^{2+}.

The PESs in Fig. 5 are computed in Jacobi coordinates where the position of the sulfur atom is varied along the coordinates R ∈ [0.5, 5] (Å) and θ ∈ [0, 90]° relative to the center of mass of O_2 (see the Supplementary Materials for more details). The oxygen atoms are separated by the equilibrium distance of the neutral O_2 ($X^3\Sigma_g^-$) ground state. Panels A and B show PES cuts and the MEPs, respectively, and present a decay pathway from the linear configuration OOS where the sulfur atom leaves the O_2 molecule by crossing the potential energy barrier in a transition from the $^1A'$ to the $^3A''$ state at around 34.5 eV, which is where the experimental data start showing a signal. The KER obtained by going to the lowest final state is about 6 eV (see table S2), which is roughly 1.5 eV more than the KER measured in the present experiments (4.7 ± 0.3 eV). The excess energy may suggest that some of the energy is converted to vibrational or rotational energy of the O_2 moiety. Another explanation could be that the sulfur ion does not end up in the ground state but instead the ^2D state, which is 1.84 eV above the ground state.

For possible examples of this proposed mechanism of O_2^+ production, we turn first to the results of Nerney and co-workers (*37*), who reviewed and updated results from Voyager, Galileo, and Cassini and found that the Io plasma torus derived from ionization of SO_2 contains several multiply charged ions. O_2^+ could very well be present but undetected, after formation by fragmentation of multiply charged SO_2. The present ionic pathway for the formation of O_2^+ may also be proposed as an alternative to the established mechanism producing O_2^+ from CO_2. For instance, Larimian and co-workers (*38*) suggested $CO_2^{2+} \rightarrow O_2^+ + C^+$ as a possible reaction path. Since CO_2^{2+} dications were detected in the outer atmospheres of those solar system bodies (*39*, *40*), the high O_2^+ concentration in the ionospheres of both Venus and Mars may have some contribution from CO_2^{2+} dissociation. Further investigations are needed for confirmation. We also note that the major dissociation channels of doubly charged SO_2 produce O^+ ions and both the reactions: $O^+ + SO_2 \rightarrow$

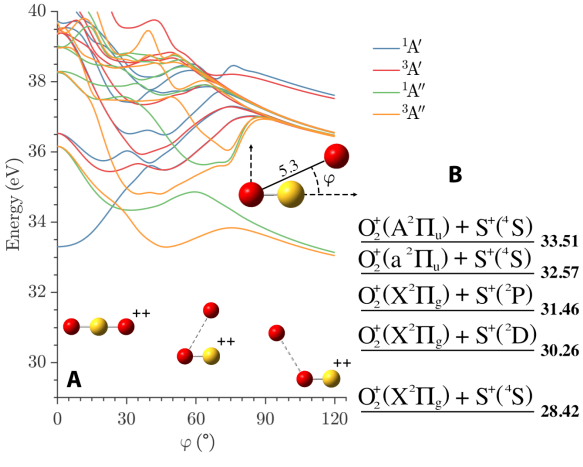

Fig. 3. Potential energy surface cuts of the lowest electronic states of SO_2^{2+} for varying angle φ. (**A**) PES cuts of the lowest electronic states of SO_2^{2+} by varying angle φ from 0° to 120°. (**B**) Thermodynamic thresholds of $O_2^+ + S^+$. The reference energy is that of SO_2 ($X\ ^1A_1$) in its vibrationless ground state. Other cuts are given in figs. S2 to S5.

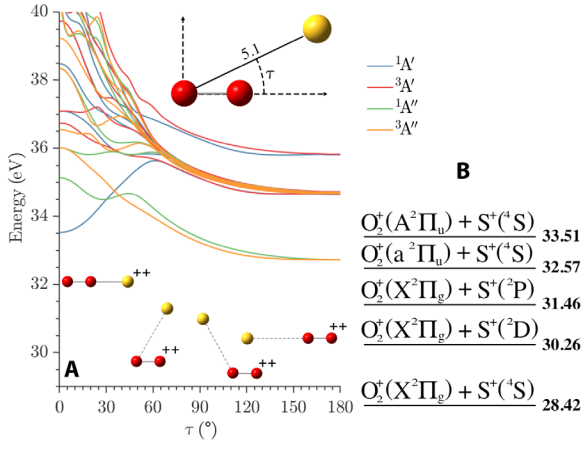

Fig. 4. Potential energy surface cuts of the lowest electronic states of SO_2^{2+} for varying angle τ. (**A**) PES cuts of the lowest electronic states of SO_2^{2+} by varying angle τ from 0° to 180°. In (**B**), the thermodynamic thresholds of $O_2^+ + S^+$ are indicated. The reference energy is that of SO_2 ($X\ ^1A_1$) in its vibrationless ground state. Other cuts are given in figs. S6 to S9.

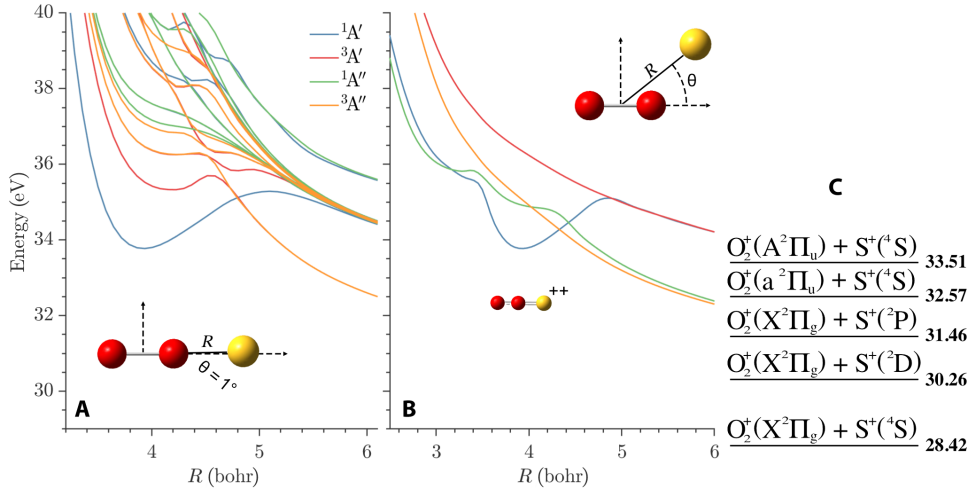

Fig. 5. Potential energy surface cuts and minimum energy paths of OOS^{2+}. (**A**) One-dimensional PES cuts of OOS^{2+} with an O—O distance at the neutral O_2 ($X^3\Sigma_g^-$) ground-state equilibrium geometry. (**B**) MEPs of OOS^{2+} with a stable $^1A'$ state in quasi-linear configuration. In (**C**), the thermodynamic thresholds of $O_2^+ + S^+$ are indicated. The reference energy is that of SO_2 ($X\ ^1A_1$) in its vibrationless ground state. Other cuts are given in figs. S6 to S9.

$O_2^+ + SO$ and $O^+ + SO_2 \rightarrow O_2 + SO^+$ are exothermic and might contribute to abiotic O_2 formation in suitable circumstances.

DISCUSSION

The present measurements tell us the fraction of double photoionization of SO_2 that leads to O_2^+ production for a range of photon energies from 40.8 eV to above the S2p and O1s inner shell thresholds (see Table 1 and Materials and Methods). As the photon energy increases, the O_2^+ fraction decreases, mainly because of competition from other dissociation pathways. The cross section for double ionization of SO_2 (*32*) is 0.5 Mb at 40 eV, rises to a peak of 1.8 Mb near 60 eV, and declines to 1 Mb by 120 eV. The cross section for S2p ionization, which is dominantly double ionization, rises strongly at the S2p threshold near 170 eV, reaches a maximum of about 4 Mb by 190 eV, and declines slowly at higher energies (*41*). Its value above the O1s edge is not known. By combining the available double-ionization cross sections with our fractions of O_2^+ formation and an estimate of the solar XUV irradiance at the relevant energies, we can estimate the rate of O_2^+ production for any planetary situation where SO_2 is present. To attempt a practical estimate, we assume that the vertical distribution of SO_2 can be represented by a single 1-cm layer at a pressure p (pressure/mbar), exposed to the full XUV flux. For the solar XUV flux, we first note the warning given by Woods *et al.* (*42*) that this flux is extremely variable on all time scales. As an estimate of average XUV irradiance at the current epoch (medium active sun), we adopt a figure of 0.1 mW m^{-2} nm^{-1} over the whole relevant range. For the specific flux at the HeIIα line and on the strong coronal lines near 180 Å, we use the figures given by Allen (*43*), which sum to an overall flux of about the same intensity as our global estimate in the low-energy range. The resulting rate of O_2^+ production k for a planet at Earth's present orbital distance is $k \geq 5 \times 10^7 p$ molecules cm^{-2} s^{-1}. Equivalently, about 2% of all the SO_2 would be converted to O_2^+ in 1 year, which is not much, but in 50 years, 100% of the original amount would be converted, if the raw SO_2 was constantly replenished. For a planet at Venus' current heliocentric distance, the rate of production would be a factor of 2 faster, while for one at the distance of Jupiter, it would be 25 times slower. For the whole Earth, the total rate of O_2^+ production would amount to about $4 \times 10^4 p$ kg per year. We note that formation of O_2^+ by the same reaction is known to be caused by electron impact double ionization (*44*) and that suitably energetic electrons and other charged particles may often be abundant in the realms where XUV penetrates. Because of this, and because we cannot include the highest photon energies, our calculated rates may well be too low and should be taken as order-of-magnitude estimates only.

Table 1. Experimentally quantified O_2^+ amount. The amount of O_2^+ formation relative to all dissociative double photoionization. Estimated from the experimental data.

hν/eV	% O_2^+
40.8	12 ± 1
88.9	2.2 ± 0.6
100	2.1 ± 0.4
170	1.1 ± 0.2
180	0.6 ± 0.1
535	0.5 ± 0.2

To estimate the yield of neutral O_2 from O_2^+, one ultimately needs a realistic atmospheric model and the rates of relevant bimolecular reactions. In addition to neutralization by free electrons and three-body recombination of the resulting O atoms, neutral O_2 can be formed efficiently by charge exchange. In the present terrestrial atmosphere, the most effective charge acceptor is NO, which is present in useful abundance in both the E and F layers [up to 400 km; see (*42*)] and for which charge exchange is highly exothermic [ionization energy (IE)(O_2) = 12.1 eV, IE(NO) = ca. 9.5 eV] (*45*). In an atmosphere dominated by volcanic outgassing of S species, both H_2S (*46*) (IE = 10.3 eV) and SO_2 itself (*47*), for which charge exchange is almost resonant (IE = 12.2 eV), would be possible partners. In some environments, NH_3 (IE = ca. 10.5 eV) could be another effective

charge exchange acceptor (*48*). Thus, we are confident that conversion from O_2^+ to O_2 will have a real positive efficiency in many atmospheric circumstances. We also note that exothermic charge transfer reactions generally have gas-kinetic cross sections and thus maximal rates [quoted in (*46*)].

Here, we report the first evidence for the direct production of O_2^+ from SO_2 doubly charged ions. We have established that O_2^+ is formed efficiently by dissociative double ionization of SO_2 induced by absorption of 30.4-nm radiation of the HeIIα line, an intense component of the solar spectrum and of many stellar spectra, as well as by several other higher solar x-ray line photon energies. We believe that the same electronic states of nascent SO_2^{2+} that lead to O_2^+ formation will be created by all forms of double ionization, whether by high-energy photon impact or by charged particle impact. The process is therefore expected to be significant in the abiotic formation of molecular oxygen in planetary atmospheres rich in SO_2, where O_2^+ can be converted to O_2 by the well-established pathways of electron recombination or charge exchange. It represents an alternative to and is expected to compete with the well-established abiotic O_2 production pathways via the photodissociation of water vapor by XUV light or the NUV photochemistry of titanium (IV) oxide (titania).

MATERIALS AND METHODS

Experimental details

Multiparticle coincidence experiments were carried out at 40.81-eV photon energy and a selection of solar soft x-ray line energies (about 88, 180, and 561 eV), which are well above the adiabatic single-photon double-ionization onset of SO_2 at 33.5 eV (*27*). The TOF-PEPEPIPICO apparatus used in the experiment has been described before (*28*, *49*). Briefly, it allows for continuous and simultaneous detection of multiple electrons with energy information and multiple cations with mass/charge information. An effusive jet of target gas is let into the interaction chamber by a hollow needle, intersecting the wavelength selected light from a pulsed discharge helium lamp for the 40.81-eV measurements and from beamline UE52 SGM of the synchrotron radiation facility BESSY-II in Berlin for the higher photon energies, respectively. Upon ionization at 40.81 eV, a weak electrostatic field in the ionization region helps guiding any near-zero electrons into a flight tube, leading to a 2.2-m distant detector. A continuous, strong divergent field from a permanent conical magnet (or a ring magnet when ions are also extracted) in the same region guides almost all photoelectrons of a wide kinetic energy range (up to a few hundred electron volts) into a much weaker, homogeneous solenoid field in the flight tube, confining the electrons onto the detector. All the electrons have sufficient energy to arrive within 10 μs. After about 150 ns when all relevant electrons have left the source region, a strong electric field is applied to extract the cations in the opposite direction, through the ring magnet. The ions are accelerated by a two-field configuration optimized for time focusing conditions. The strength of the draw-out pulse and the associated acceleration field determine the mass resolution and the time width of signals for fragment ions formed with more than thermal kinetic energy. The draw-out pulse field affects the detectability of ion pairs of equal mass-to-charge ratio (m/z) such as $O^+ + O^+$ or $O_2^+ + S^+$ because the ion detector and associated electronics used in these experiments imposed a deadtime of 25 ns. At the time of the experiments, the collection-detection efficiency was about 30% for electrons and 10% for ions at $m/z = 100$. Because the final ion energy at the detector was less than 2 keV, the efficiency was somewhat higher for lighter ions. Electron kinetic energy resolution ($E/\Delta E$) was about 20 throughout, while mass resolution ranged from 30 to 100 (FWHM) according to the strength of the draw-out pulse; all ions of interest from SO_2 except equal mass pairs were fully resolved under all conditions, but the ^{34}S isotopic variants were only partially resolved. Also, because the higher photon energies typically led to substantially higher electron kinetic energies, which are more difficult to resolve, the BESSY-II experiments were primarily restricted to ion-ion coincidence measurements in DC mode.

Error bars included in the graphical and tabular presentations of the experimental data represent ±1σ deviations derived from the numbers of coincidence counts involved, with due attention to propagation of errors on the assumptions that errors in combining quantities such as numerators and denominators are uncorrelated and that the data are drawn from a normally distributed parent population, following the concepts of Bevington (*50*).

Computational details

All the ab initio electronic structure calculations on different levels of theory were performed using the MOLPRO program suite (*51*). In the present study, we mapped the three-dimensional PESs of SO_2^{2+} for the six lowest A′ and six lowest A″ of singlet and triplet spin multiplicities using Jacobi coordinates. The PESs have been generated using the complete active space self-consistent field (CASSCF) (*52*, *53*) approach followed by the internally contracted multireference configuration interaction (MRCI) method (*54*–*56*). The CASSCF active space constitutes the whole set of all configurations, which is allowing all the possible excitations of all valence electrons in valence orbitals. The electronic states having the same spin multiplicity are computed according to the state-average procedure, as implemented in MOLPRO. For the MRCI calculations, all configurations having a coefficient greater than 0.005 in the CI expansion of the CASSCF wave functions were taken into account as a reference. The computations were done in the C_s point group with wave functions leading to more than 7×10^8 uncontracted configurations for the singlet electronic states. For the triplet electronic states, we considered more than 26×10^8 uncontracted configurations. For these calculations, the aug-cc-pV(Q+d)Z and the aug-cc-pVQZ basis sets of Dunning and co-workers were used to describe the S and O atoms, respectively (*57*–*59*). Adding the tight-d functions to describe the sulfur atom improves the accuracy of the results as shown in different works [e.g., in (*60*) and references therein]. Furthermore, to evaluate the energies of the dissociation limits of SO_2^{2+} forming $[S + O_2]^{2+}$, the partially spin-restricted coupled cluster method including perturbative treatment of triple excitation [RCCSD(T)] (*61*–*63*) is used. For the RCCSD(T) computations, we used the aug-cc-pV(5+d)Z basis set for sulfur and the aug-cc-pV5Z for oxygen. The energetics presented in this work were computed typically with an accuracy of about ±0.05 eV as known from benchmark calculations (*28*, *64*).

SUPPLEMENTARY MATERIALS

Supplementary material for this article is available at https://science.org/doi/10.1126/sciadv.abq5411

REFERENCES AND NOTES

1. H. D. Holland, The oxygenation of the atmosphere and oceans. *Philos. Trans. R. Soc. Lond. B Biol. Sci.* **361**, 903–915 (2006).
2. J. F. Kasting, J. B. Pollack, D. Crisp, Effects of high co2 levels on surface temperature and atmospheric oxidation state of the early earth. *J. Atmos. Chem.* **1**, 403–428 (1984).

3. J. F. Kasting, J. C. G. Walker, Limits on oxygen concentration in the prebiological atmosphere and the rate of abiotic fixation of nitrogen. *J. Geophys. Res. Oceans* **86**, 1147–1158 (1981).
4. J. F. Kasting, S. C. Liu, T. M. Donahue, Oxygen levels in the prebiological atmosphere. *J. Geophys. Res. Oceans* **84**, 3097–3107 (1979).
5. F. Tian, K. France, J. L. Linsky, P. J. D. Mauas, M. C. Vieytes, High stellar fuv/nuv ratio and oxygen contents in the atmospheres of potentially habitable planets. *Earth Planet. Sci. Lett.* **385**, 22–27 (2014).
6. R. Wordsworth, R. Pierrehumbert, Abiotic oxygen-dominated atmospheres on terrestrial habitable zone planets. *Astrophys. J. Lett.* **785**, L20 (2014).
7. R. Luger, R. Barnes, Extreme water loss and abiotic o2 buildup on planets throughout the habitable zones of m dwarfs. *Astrobiology* **15**, 119–143 (2015).
8. N. Narita, T. Enomoto, S. Masaoka, N. Kusakabe, Titania may produce abiotic oxygen atmospheres on habitable exoplanets. *Sci. Rep.* **5**, 13977 (2015).
9. Z. Lu, Y. C. Chang, Q.-Z. Yin, C. Y. Ng, W. M. Jackson, Evidence for direct molecular oxygen production in CO_2 photodissociation. *Science* **346**, 61–64 (2014).
10. J. Li, M. S. Gudipati, Y. L. Yung, The influence of europa's plumes on its atmosphere and ionosphere. *Icarus* **352**, 113999 (2020).
11. Z. Li, M. Zhao, T. Xie, Z. Luo, Y. Chang, G. Cheng, J. Yang, Z. Chen, W. Zhang, G. Wu, X. Wang, K. Yuan, X. Yang, Direct observation of the C + S_2 channel in CS_2 photodissociation. *J. Phys. Chem. Lett.* **12**, 844–849 (2021).
12. X.-D. Wang, X.-F. Gao, C.-J. Xuan, S. X. Tian, Dissociative electron attachment to co2 produces molecular oxygen. *Nat. Chem.* **8**, 258–263 (2016).
13. A. F. Nagy, R. W. Schunk, *Encyclopedia of Physical Science and Technology* (Academic Press, ed. 3, 2002).
14. C. Y. Na, L. W. Esposito, T. E. Skinner, International ultraviolet explorer observation of Venus SO_2 and SO. *J. Geophys. Res. Atmos.* **95**, 7485–7491 (1990).
15. E. Barker, Detection of SO_2 in the UV spectrum of Venus. *Geophys. Res. Lett.* **6**, 117–120 (1979).
16. E. Lellouch, M. A. McGrath, K. L. Jessup, Io's atmosphere, in *Io After Galileo*, R. M. C. Lopes, J. R. Spencer, Eds. (Springer-Praxis, 2007).
17. R. Hu, S. Seager, W. Bains, Photochemistry in terrestrial exoplanet atmospheres. II. H_2S and SO_2 photochemistry in anoxic atmospheres. *Astrophys. J.* **769**, 6 (2013).
18. J. Farquhar, H. Bao, M. Thiemens, Atmospheric influence of Earth's earliest sulfur cycle. *Science* **289**, 756–758 (2000).
19. A. L. Broadfoot, M. J. S. Belton, P. Z. Takacs, B. R. Sandel, D. E. Shemansky, J. B. Holberg, J. M. Ajello, S. K. Atreya, T. M. Donahue, H. W. Moos, J. L. Bertaux, J. E. Blamont, D. F. Strobel, J. C. McConnell, A. Dalgarno, R. Goody, M. B. McElroy, Extreme ultraviolet observations from voyager 1 encounter with jupiter. *Science* **204**, 979–982 (1979).
20. L. Kaltenegger, D. Sasselov, Detecting planetary geochemical cycles on exoplanets: Atmospheric signatures and the case of SO_2. *Astrophys. J.* **708**, 1162–1167 (2009).
21. X. Zhang, M.-C. Liang, F. Montmessin, J.-L. Bertaux, C. Parkinson, Y. L. Yung, Photolysis of sulphuric acid as the source of sulphur oxides in the mesosphere of Venus. *Nat. Geosci.* **3**, 834–837 (2010).
22. J. Pearl, R. Hanel, V. Kunde, W. Maguire, K. Fox, S. Gupta, C. Ponnamperuma, F. Raulin, Identification of gaseous so2 and new upper limits for other gases on io. *Nature* **280**, 755–758 (1979).
23. C. T. Russell, M. G. Kivelson, Detection of so in io's exosphere. *Science* **287**, 1998–1999 (2000).
24. L. Kaltenegger, W. Henning, D. Sasselov, Detecting vocanism on extrasolar planets. *Astrophys. J.* **140**, 1370 (2010).
25. S. Ranjan, Z. R. Todd, J. D. Sutherland, D. D. Sasselov, Sulfidic anion concentrations on early earth for surficial origins-of-life chemistry. *Astrobiology* **18**, 1023–1040 (2018).
26. K. Lin, X. Hu, S. Pan, F. Chen, Q. Ji, W. Zhang, H. Li, J. Qiang, F. Sun, X. Gong, H. Li, P. Lu, J. Wang, Y. Wu, J. Wu, Femtosecond resolving photodissociation dynamics of the SO_2 molecule. *J. Phys. Chem. Lett.* **11**, 3129–3135 (2020).
27. M. Hochlaf, J. H. D. Eland, A theoretical and experimental study of the SO_2^{2+} dication. *J. Chem. Phys.* **120**, 6449–6460 (2004).
28. M. Jarraya, M. Wallner, G. Nyman, S. Ben Yaghlane, M. Hochlaf, J. H. D. Eland, R. Feifel, State selective fragmentation of doubly ionized sulphur dioxide. *Sci. Rep.* **11**, 17137 (2021).
29. T. A. Field, J. H. D. Eland, Fragmentation dynamics of SO_2^{2+}. *Int. J. Mass Spectrom.* **192**, 281–288 (1999).
30. L. Chen, C. Lee, Y. Lee, Isomers of SO_2: Infrared absorption of SOO in solid argon. *J. Chem. Phys.* **105**, 9454–9460 (1996).
31. D. M. Curtis, J. H. D. Eland, Coincidence studies of doubly charged ions formed by 30.4 nm photoionization. *Int. J. Mass Spectrom. Ion Processes* **63**, 241–264 (1985).
32. T. Masuoka, Kinetic-energy release and intercharge distance of the sulfur dioxide dication (SO_2^{2+}). *Int. J. Mass Spectrom.* **209**, 125–131 (2001).
33. J. H. D. Eland, F. S. Wort, R. N. Royds, A photoelectron-ion-ion triple coincidence technique for the study of double photoionization and its consequences. *J. Electron. Spectros. Relat. Phenomena* **41**, 297–309 (1986).
34. J. H. D. Eland, The dynamics of three-body dissociations of dications studied by the triple coincidence technique pepipico. *Mol. Phys.* **61**, 725–745 (1987).
35. S. Hsieh, J. H. D. Eland, Charge separation reaction dynamics from pepipico using a position-sensitive detector. *Rapid Commun. Mass Spectrom.* **9**, 1261–1265 (1995).
36. S. Hsieh, J. H. D. Eland, Reaction dynamics of three-body dissociations in triatomic molecules from single-photon double ionization studied by a time- and position-sensitive coincidence method. *J. Phys. B At. Mol. Opt. Phys.* **30**, 4515–4534 (1997).
37. E. G. Nerney, F. Bagenal, A. Steffi, Io plasma torus ion composition: Voyager, Galileo, and Cassini. *J. Geophys. Res. Space Physics* **122**, 727–744 (2017).
38. S. Larimian, S. Erattupuzha, S. Mai, P. Marquetand, L. Gonzalez, A. Baltuska, M. Kitzler, X. Xie, Molecular oxygen observed by direct photoproduction from carbon dioxide. *Phys. Rev. A* **95**, 011404 (2017).
39. H. Gu, J. Cui, D. Niu, L. Dai, J. Huang, X. Wu, Y. Hao, Y. Wei, Observation of CO_2^{++} dication in the dayside martian upper atmosphere. *Earth Planet. Phys.* **4**, 396–402 (2020).
40. A. Beth, K. Altwegg, H. Balsiger, J.-J. Berthelier, M. R. Combi, J. De Keyser, B. Fiethe, S. A. Fuselier, M. Galand, T. I. Gombosi, M. Rubin, T. Sémon, Rosina ion zoo at comet 67P. *A&A* **642**, A27 (2020).
41. G. Cooper, E. B. Zarate, R. K. Jones, C. Brion, Absolute oscillator strengths for photoabsorption, photoionization and ionic photofragmentation of sulphur dioxide. II. The S 2p and 2s inner shells. *Chem. Phys.* **150**, 251–261 (1991).
42. T. N. Woods, P. C. Chamberlin, W. K. Peterson, R. R. Meier, P. G. Richards, D. J. Strickland, G. Lu, L. Qian, S. C. Solomon, B. A. Iijima, A. J. Mannucci, B. T. Tsurutani, Xuv photometer system (xps): Improved solar irradiance algorithm using chianti spectral models. *Sol. Phys.* **250**, 235–267 (2008).
43. C. W. Allen, *Astrophysical Quantities* (The Athlone Press, ed. 3, 1976), pp. 178 and 195.
44. J. D. Fletcher, M. A. Parkes, S. D. Price, Electron ionisation of sulfur dioxide. *Chem. Phys.* **138**, 184309 (2013).
45. N. S. Shuman, D. E. Hunton, A. A. Viggiano, Ambient and modified atmospheric ion chemistry: From top to bottom. *Chem. Rev.* **115**, 4542–4570 (2015).
46. D. Smith, N. G. Adams, T. M. Miller, A laboratory study of the reactions of n+, n2+, n3+, n4+, o+, o2+, and no+ ions with several molecules at 300k. *Chem. Phys.* **69**, 308–318 (1978).
47. H. Böhringer, M. Durup-Ferguson, D. W. Fahey, F. C. Fehsenfeld, E. E. Ferguson, Collisional relaxation of vibrationally excited o2+ ions. *Chem. Phys.* **79**, 4201–4213 (1983).
48. D. K. Bohme, F. C. Fehsenfeld, Thermal reactions of O_2^+ and O- ions in gaseous ammonia. *Can. J. Chem.* **47**, 2715–2717 (1969).
49. J. H. Eland, R. Feifel, Double ionisation of icn and brcn studied by a new photoelectron-photoion coincidence technique. *Chem. Phys.* **327**, 85–90 (2006).
50. P. R. Bevington, *Data Reduction and Error Analysis for the Physical Sciences* (MrGraw Hill, 1969).
51. H.-J. Werner, P. J. Knowles, G. Knizia, F. R. Manby, M. Schütz, P. Celani, W. Györffy, D. Kats, T. Korona, R. Lindh, Molpro, version 2019.2, a package of ab initio programs (2019).
52. P. J. Knowles, H.-J. Werner, An efficient second-order mc scf method for long configuration expansions. *Chem. Phys. Lett.* **115**, 259–267 (1985).
53. H. Werner, P. J. Knowles, A second order multiconfiguration scf procedure with optimum convergence. *Chem. Phys.* **82**, 5053–5063 (1985).
54. H. Werner, P. J. Knowles, An efficient internally contracted multiconfiguration-reference configuration interaction method. *Chem. Phys.* **89**, 5803–5814 (1988).
55. P. J. Knowles, H.-J. Werner, An efficient method for the evaluation of coupling coefficients in configuration interaction calculations. *Chem. Phys. Lett.* **145**, 514–522 (1988).
56. K. R. Shamasundar, G. Knizia, H.-J. Werner, A new internally contracted multi-reference configuration interaction method. *Chem. Phys.* **135**, 054101 (2011).
57. R. A. Kendall, T. H. Dunning, R. J. Harrison, Electron affinities of the first-row atoms revisited. Systematic basis sets and wave functions. *J. Chem. Phys.* **96**, 6796–6806 (1992).
58. D. E. Woon, T. H. Dunning, Gaussian basis sets for use in correlated molecular calculations. iii. The atoms aluminum through argon. *J. Chem. Phys.* **98**, 1358–1371 (1993).
59. T. H. Dunning, K. A. Peterson, A. K. Wilson, Gaussian basis sets for use in correlated molecular calculations. x. The atoms aluminum through argon revisited. *Chem. Phys.* **114**, 9244–9253 (2001).
60. T. Trabelsi, M. M. Al-Mogren, M. Hochlaf, J. S. Francisco, Mechanistic study of the photoexcitation, photoconversion, and photodissociation of cs2. *Chem. Phys.* **149**, 064304 (2018).
61. C. Hampel, K. A. Peterson, H. Werner, A comparison of the efficiency and accuracy of the quadratic configuration interaction (qcisd), coupled cluster (ccsd), and brueckner coupled cluster (bccd) methods. *Chem. Phys. Lett.* **190**, 1–12 (1992).
62. M. J. O. Deegan, P. J. Knowles, Perturbative corrections to account for triple excitations in closed and open shell coupled cluster theories. *Chem. Phys. Lett.* **227**, 321–326 (1994).
63. P. J. Knowles, C. Hampel, H.-J. Werner, Erratum: "Coupled cluster theory for high spin, open shell reference wave functions" [j. chem. phys. 99, 5219 (1993)]. *Chem. Phys.* **112**, 3106–3107 (2000).
64. M. Hochlaf, Advances in spectroscopy and dynamics of small and medium sized molecules and clusters. *Phys. Chem. Chem. Phys.* **19**, 21236–21261 (2017).

Acknowledgments: This work was carried out while M.H. was Waernska Guest Professor at the University of Gothenburg. We thank the Helmholtz Zentrum Berlin for the allocation of synchrotron radiation beam time and the staff of BESSY-II for smooth operation of the storage ring in single-bunch mode. We thank K. Franzreb from Arizona State University and M. Sundin from the University of Gothenburg for encouraging feedback on this work. M.W. thanks V. Zhaunerchyk from the University of Gothenburg for interesting discussions. **Funding:** We thank the Swedish Research Council (VR; grant numbers 2018-03731 and 2020-05293) and the Knut and Alice Wallenberg Foundation, Sweden (grant number 2017.0104) for financial support. The computations involved the Swedish National Infrastructure for Computing (SNIC) at the Chalmers Centre for Computational Science and Engineering (C3SE) partially funded by the Swedish Research Council (VR) through grant number 2018-05973. The authors are also grateful for financial support from the Programme National "Physique et Chimie du Milieu Interstellaire" (PCMI) of the Centre National de la Recherche Scientifique (CNRS)/Institut National des Sciences de l'Univers (INSU) and the Institut de Chimie (INC)/Institut de Physique (INP), co-funded by the Commissariat à l'Energie Atomique (CEA) and Centre National d'Etudes Spatiales (CNES). The research leading to these results has received funding from the European Union's Horizon 2020 research and innovation programme under grant agreement number 730872. This article is based upon work from COST Action CA17120 - Chemobrionics, supported by COST [European Cooperation in Science and Technology (http://www.cost.eu)]. **Author contributions:** J.H.D.E. and R.F. devised the experimental setup. J.H.D.E., R.F., M.W., E.O., V.I., and R.J.S. conducted the experimental research. J.H.D.E. and M.W. performed the data analysis. M.W., M.J., S.B.Y., and M.H. carried out the calculations. M.W., J.H.D.E., M.H., and R.F. wrote the first draft of the manuscript. All authors discussed the results and contributed to the manuscript at several instances. **Competing interests:** The authors declare that they have no competing interests. **Data and materials availability:** All data needed to evaluate the conclusions in the paper are present in the paper and/or the Supplementary Materials.

Submitted 14 April 2022
Accepted 6 July 2022
Published 19 August 2022
10.1126/sciadv.abq5411